NeuroImage 49 (2010) 3187–3197

Contents lists available at ScienceDirect

NeuroImage

journal homepage: www.elsevier.com/locate/ynimg

Combining functional and anatomical connectivity reveals brain networks for auditory language comprehension

Dorothee Saur [a,c,*], Björn Schelter [c,d,e], Susanne Schnell [b,c], David Kratochvil [a,c], Hanna Küpper [a,c], Philipp Kellmeyer [a,c], Dorothee Kümmerer [a,c], Stefan Klöppel [c], Volkmar Glauche [a,c], Rüdiger Lange [a,c], Wolfgang Mader [a,c,d,e], David Feess [a,c,d,e], Jens Timmer [d,e,f], Cornelius Weiller [a,c]

[a] Department of Neurology, Medical Physics, University Medical Center Freiburg, Breisacher Strasse 64, D-79106 Freiburg, Germany
[b] Department of Diagnostic Radiology, Medical Physics, University Medical Center Freiburg, Breisacher Strasse 64, D-79106 Freiburg, Germany
[c] Freiburg Brain Imaging, University Medical Center Freiburg, Breisacher Strasse 64, D-79106 Freiburg, Germany
[d] Freiburg Center for Data Analysis and Modeling, Eckerstraße 1, D-79104 Freiburg, Germany
[e] Department of Physics, University Freiburg, Hermann-Herder-Str. 3, D-79104 Freiburg, Germany
[f] Freiburg Institute for Advanced Studies, Albertstraße 19, D-79104 Freiburg, Germany

ARTICLE INFO

Article history:
Received 29 July 2009
Revised 30 September 2009
Accepted 4 November 2009
Available online 12 November 2009

Keywords:
fMRI
DTI
Directed partial correlation
Tractography
Language networks

ABSTRACT

Cognitive functions are organized in distributed, overlapping, and interacting brain networks. Investigation of those large-scale brain networks is a major task in neuroimaging research.
Here, we introduce a novel combination of functional and anatomical connectivity to study the network topology subserving a cognitive function of interest. (i) In a given network, direct interactions between network nodes are identified by analyzing functional MRI time series with the multivariate method of directed partial correlation (dPC). This method provides important improvements over shortcomings that are typical for ordinary (partial) correlation techniques. (ii) For directly interacting pairs of nodes, a region-to-region probabilistic fiber tracking on diffusion tensor imaging data is performed to identify the most probable anatomical white matter fiber tracts mediating the functional interactions. This combined approach is applied to the language domain to investigate the network topology of two levels of auditory comprehension: lower-level speech perception (i.e., phonological processing) and higher-level speech recognition (i.e., semantic processing).
For both processing levels, dPC analyses revealed the functional network topology and identified central network nodes by the number of direct interactions with other nodes. Tractography showed that these interactions are mediated by distinct ventral (via the extreme capsule) and dorsal (via the arcuate/superior longitudinal fascicle fiber system) long- and short-distance association tracts as well as commissural fibers. Our findings demonstrate how both processing routines are segregated in the brain on a large-scale network level. Combining dPC with probabilistic tractography is a promising approach to unveil how cognitive functions emerge through interaction of functionally interacting and anatomically interconnected brain regions.

Introduction

Cognitive functions are organized in large-scale brain networks of functionally interacting and anatomically interconnected brain regions (Mesulam, 1990). These large-scale networks are composed of distributed cortical grey matter regions which functionally interact through long- and short-distance white matter fiber tracts.

In this study, we introduce a novel combination of functional (i.e., directed partial correlation, dPC) and anatomical (i.e., region-to-region probabilistic tractography) connectivity which enables us to infer the organization of cognitive large-scale brain networks from functional MRI (fMRI) and diffusion tensor imaging (DTI) data.

To analyze the functional network structure underlying fMRI data, different approaches are conceivable. On the one hand, analytic routines that are chiefly hypothesis-based like dynamic causal modeling have been introduced by Friston et al. (2003) and used in a number of studies investigating cognitive functions such as language (e.g., Bitan et al., 2005; Heim et al., 2009; Leff et al., 2008; Mechelli et al., 2005). On the other hand, strategies allowing for a more hypothesis-free exploration might be advantageous in cases where such prior knowledge of the putative functional network structure is scarce. Here, we used the multivariate method of dPC (Eichler, 2005; Mader et al., 2008) which falls into the second class of hypothesis-free approaches. In a given network, dPC is capable of detecting direct

* Corresponding author. Department of Neurology, University Medical Center Freiburg, Breisacher Strasse 64, 79106 Freiburg, Germany. Fax: +49 761 2705416.
E-mail address: dorothee.saur@uniklinik-freiburg.de (D. Saur).

1053-8119/$ – see front matter © 2009 Elsevier Inc. All rights reserved.
doi:10.1016/j.neuroimage.2009.11.009

interactions between network nodes. It implements the concept of Granger causality (Granger, 1969) which, in principle, allows for the detection of the direction of information flow by taking the past of the processes into account. Owing to the temporal characteristics of the fMRI time series, however, it is still questionable to which extent causal inferences from fMRI data are possible (Roebroeck et al., 2005). Still, the reason for using dPC as a causal inference method is that taking into account the past of the processes protects against false-positive/negative conclusions which might result from ordinary correlation-based techniques (see below).

To identify the most probable interconnecting white matter pathways for pairs of directly interacting nodes, we used a region-to-region probabilistic tractography (Kreher et al., 2008b). Thus, prior functional network analysis by means of dPC restricts the fiber tracking to those connections which turned out to be functionally most relevant.

Once the network nodes are defined by fMRI, the dPC analysis and the fiber tracking procedure are both completely data-driven, thus no *a priori* hypothesis concerning the functional network structure as well as the spatial course of the white matter fiber tracts is necessary. We propose that in conjunction, these complementary methods allow for the identification of the major functional and structural determinates subserving a specific cognitive function of interest.

In this study, this combined approach is applied to the language domain to describe large-scale networks subserving auditory comprehension. In an fMRI event-related experiment, we attempt to map key regions involved in lower-level speech perception, mainly attributable to phonological processing (i.e., decoding phonetic properties) and higher-level speech recognition, mainly attributable to lexical–semantic processing (i.e., extracting and elaborating meaning). The resulting sets of key regions represent the nodes of the networks, which will subsequently be studied concerning their functional and anatomical network topology.

Methods

Subjects

Thirty-three native German speakers (22 males, mean age 34 yr, range 18–71 yr, 18 right-handed) participated in the study. Left-handed subjects were included to facilitate bilateral language activation for bilateral network analysis (see below). All subjects were scanned with the approval of the local ethics committee and gave their written consent.

fMRI: Stimuli and experimental design

Stimuli

The auditory sentence comprehension task consisted of 90 stimuli of meaningful speech (SP), pseudo speech (PS) and reversed speech (REV) resulting in a total of 270 stimuli. SP and PS stimuli are identical with the stimuli used in Saur et al. (2008).

The meaningful sentences were composed of well-formed German sentences which all had the same subject–verb–object structure, e.g., "Der Pilot fliegt das Flugzeug" (in English, "The pilot flies the plane"). The pseudo sentences were derived from the normal sentences by substituting phonemes on the basis of German phonotactical rules resulting in meaningless sentences with a preserved German sound structure, e.g., "Ren Simot plieft mas Kugireug" (English translation not possible). Pseudo sentences match the original sentences in length, syllable structure, and phonemic complexity, and intonation was as natural as possible.

The reversed stimuli were obtained by playing the pseudo sentences in reverse resulting in unintelligible stimuli which have a disturbed sound structure but the same frequency spectrum like pseudo sentences. Basically, time-reversed sentences sound like a strange, unknown foreign language.

Based on these properties, we discriminate two levels of auditory language comprehension. A lower level of speech perception is defined by contrasting pseudo with reversed speech. This level should mainly be attributable to phonological processing because the basic phonemic sound structure is preserved in pseudo but not in reversed speech. In contrast, a higher level of speech recognition is defined by contrasting speech with pseudo speech. This level should mainly be associated with semantic processing since meaning is preserved in speech but not in pseudo speech.

Sentences were spoken by a female voice and recorded with the commercial software GoldWave with a sampling rate of 16 kHz and 16-bit resolution. Reversed speech was generated using the same software.

Experimental design

Stimuli were presented in an event-related design and distributed over three sessions. Within each session, the order of sentences was pseudo-randomized, with pairs of normal, pseudo, or reversed sentences never occurring in the same session. The duration of the stimuli ranged from 1500 to 3000 ms, the interstimulus interval varied between 3000 and 6000 ms. The order of sessions was randomized across participants.

Task and stimulus presentation

Subjects were asked to listen carefully to all stimuli and press a button at the end of each stimulus, irrespective of whether they had heard a normal, pseudo, or reversed sentence. This simple task was chosen to keep executive task demands constantly low across stimuli. Stimuli were presented binaurally with the software Presentation (http://nbs.neuro-bs.com) with MR-compatible headphones. During scanning, subjects kept their eyes open.

MRI data acquisition

Structural and functional MRI was performed in one scanning session on a 3-T TIM Trio scanner (Siemens, Erlangen, Germany) with a standard head coil.

Functional MRI

A total of 260 scans per session with 36 axial slices covering the whole brain was acquired in interleaved order using a gradient echo echo-planar (EPI) T2*-sensitive sequence (voxel size = $3\times3\times3$ mm^3, matrix = 64×64 pixel^2, TR = 2.19 s, TE = 30 ms, flip angle = 75°).

Diffusion-weighted imaging (DWI)

We acquired a total of 70 scans with 69 slices using a diffusion sensitive spin-echo EPI sequence with CSF suppression (61 diffusion encoding gradient directions [*b*-factor = 1000 s/mm], 9 scans without diffusion weighing, voxel size = $2\times2\times2$ mm^3, matrix size = 104×104 pixel^2, TR = 11.8 s, TE = 96 ms, TI = 2.3 s).

During reconstruction, both fMRI and DWI scans were corrected for motion and distortion artifacts based on a reference measurement (Zaitsev et al., 2004).

MP-RAGE

An additional high-resolution T1 anatomical scan was obtained (160 slices, voxel size = $1\times1\times1$ mm^3, matrix = 240×240 pixel^2, TR = 2.2 s, TE = 2.6 ms) for spatial processing of the fMRI and DTI data.

In total, the scanning procedure took about 60 minutes per subject.

fMRI data analysis

Statistical parametric mapping

Preprocessing. Data were analyzed using statistical parametric mapping (SPM5, http://www.fil.ion.ucl.ac.uk/spm/software/spm5/).

All slices were corrected for different acquisition times of signals by shifting the signal measured in each slice relative to the acquisition of the middle slice. Resulting volumes were spatially normalized to the Montreal Neurological Institute (MNI) reference brain using the normalization parameters estimated during segmentation of the coregistered T1 anatomical scan (Ashburner and Friston, 2005). All normalized images were then smoothed using an isotropic 9-mm Gaussian kernel to account for intersubject differences.

Statistical analysis. At first level, the three conditions SP, PS, and REV were modeled as separate regressors. Realignment parameters were included as covariates of no interest. Onset and duration of stimuli were convolved with a canonical hemodynamic response function (HRF) as implemented in SPM5. Voxel-wise regression coefficients for the three conditions were estimated using weighted least squares. Our research questions were addressed in a second level random effects analysis for which the contrast images of the three conditions were entered into a factorial design with the factors subjects and conditions. Correction for non-sphericity resulting from unequal variances between subjects and conditions was implemented. With respect to our hypotheses, we computed the differential effects between listening to pseudo versus reversed speech (i.e., phonological processing) and meaningful versus pseudo speech (i.e., semantic processing). From these contrasts, we selected peak activations (see below) which defined the nodes of the networks to be analyzed.

Directed partial correlation (dPC)

Concept of dPC

DPC (Eichler, 2005; Mader et al., 2008) is an approach in the time domain quantifying Granger causality, which enables a hypothesis-free exploration of networks in the sense that once the network nodes are defined, no further prior assumptions about the functional network structure are necessary. The concept of Granger causality is well established in the literature with several approaches to quantify it (Baccala and Sameshima, 2001; Dhamala et al., 2008; Kayser et al., 2009; Keil et al., 2009; Roebroeck et al., 2005). In terms of the analysis technique, dPC is one of many equivalent Granger causality measures in the time domain.

Granger causality is defined for multidimensional systems and is based on the common sense conception that causes precede their effects in time. Conceptually speaking, a process A is Granger causal to another process B if taking into account the past of process A helps to improve the predictability of the current state of process B. Granger himself additionally introduced the concept of instantaneous causality or instantaneous interaction. These interactions are bidirectional as the cause cannot be distinguished from the effect based on predictability. These instantaneous interactions are usually inferred from the covariance matrix of the stochastic term in autoregressive modeling, which is used to model Granger causality. By making inference purely on these covariance matrices, all causal effects are disregarded in the analysis. As done in other studies using Granger causality-based techniques in fMRI (Kayser et al., 2009; Roebroeck et al., 2005), one could use the full information of the analysis to identify causal effects. However, owing to the temporal characteristics of the fMRI time series, we restricted the dPC analyses to instantaneous interactions.

Technical description of dPC

In linear theory, the concept of Granger causality is usually modeled by vector autoregressive (VAR[p]) processes (Eq. (1)).

$$x(t) = \sum_{j=1}^{p} A(j)x(t-j) + \varepsilon(t). \tag{1}$$

In Eq. (1), the actual state x at time point t is derived from its past p states with additional input from a Gaussian white noise process $\varepsilon(t)$ with mean zero and covariance matrix Σ. The matrices $A(j)$ weigh the influence of the past states onto the actual state. Non-zero entries in the j-th matrix indicate Granger causal influences at time lag j, while zeros represent their absence.

dPC is defined by

$$\pi_{ij}(\tau) = \frac{A_{ij}(\tau)}{\sqrt{\Sigma_{ii}\rho_{ij}(\tau)}} \tag{2}$$

with

$$\rho_{ij}(\tau) = \Sigma_{ij}^{-1} + \sum_{v=1}^{\tau-1}\sum_{k,l} A_{kj}(v)\Sigma_{kl}^{-1}A_{lj}(v) + \frac{A_{ij}^2(\tau)}{\Sigma_{ii}}. \tag{3}$$

For the time lag $\tau = 0$, (2) simplifies to

$$\pi_{ij}(0) = \frac{\Sigma_{ij}}{\sqrt{\Sigma_{ii}\Sigma_{jj}}}. \tag{4}$$

Eq. (4) represents instantaneous direct influences. Owing to the poor temporal resolution in fMRI time series, such instantaneous interactions must be hypothesized for fMRI time series analysis. Eq. (4), however, differs from that for ordinary correlation based analysis as dPC analysis takes the processes' own past into account. This avoids false-positive/negative conclusions about the network structure that are due to the temporal correlation within time series themselves.

Selection of network nodes

As described above, dPC is hypothesis-free in the sense that no *a priori* assumptions concerning the interaction structure are necessary. However, the nodes of the network have to be selected first. Here we selected the major language-relevant activation peaks in the PS versus REV and SP versus PS contrast (Tables 1a/b). These activation peaks defined the nodes of four independent networks in the left and right hemispheres (see Results). Peaks in the frontal pole (superior frontal gyrus, SFG), dorsolateral prefrontal cortex (middle frontal gyrus, MFG), supplementary motor area (SMA), and the right primary motor cortex (M1) were not included into the analysis as activation in these areas is most likely attributable to language-unspecific executive demands (Table 1b).

Identical coordinates were used for time series extraction in all subjects. To prevent false-positive results due to the smoothness of the fMRI data, selected nodes had a minimum distance of at least two times the width of the smoothing kernel (i.e., 18 mm) to all neighboring nodes.

Preprocessing of time series for dPC analysis

From these coordinates, BOLD time series were extracted in each subject from the fully preprocessed but unfiltered data and averaged within a sphere of 4-mm radius. To eliminate the scanner drift, a third-degree polynomial was fitted to each of the averaged time

Table 1a
fMRI data pseudo speech>reversed speech.

Region	Coordinates	*t* value	Seed
Phonology: pseudo>reversed speech			
Left temporal			
Anterior STG	−57 0 −9	8.09	T1a
Posterior STG	−57 −33 0	7.42	T2p
Left frontal			
IFG, pars opercularis (BA 44)	−51 15 18	6.12	F3op
IFG, deep frontal operculum	−39 30 3	5.56	FOP
Precentral gyrus (dorsal premotor cortex, BA 6)	−51 −3 48	5.17	PMd

$p<0.05$ corrected ($t>5.1$).
STG, superior temporal gyrus; IFG, inferior frontal gyrus.

Table 1b
fMRI data: normal speech versus pseudo speech.

Region	Coordinates	*t* value	Seed
SEMANTICS: speech>pseudo speech			
Left temporal			
Posterior MTG	−48 −60 18	10.11	T2p
Anterior MTG	−51 0 −18	9.70	T2a
Fusiform gyrus	−30 −33 −18	8.37	FUS
Left frontal			
IFG, pars triangularis (BA 45)	−48 27 12	8.95	F3tri
IFG, pars orbitalis (BA 47)	−45 27 −12	8.83	F3orb
Middle frontal gyrus	−39 18 30	7.01	No seed
Superior frontal gyrus (frontal pole)	−9 63 27	8.41	No seed
Supplementary motor area	−3 18 54	7.24	No seed
Right temporal			
Anterior MTG	51 −3 −18	7.62	T2a
Posterior MTG	42 −54 18	5.77	T2p
Fusiform gyrus	33 −30 −21	5.40	FUS
Right frontal			
IFG, pars orbitalis	48 24 −9	6.07	F3orb
IFG, pars triangularis	54 24 9	3.63*	F3tri
Middle frontal gyrus	51 30 30	5.24	No seed
Central sulcus	42 −21 54	6.59	No seed

$p<0.05$ corrected ($t>5.1$).
*$p<0.001$ uncorrected ($t>3,2$).
MTG, middle temporal gyrus.

series. In each single subject, the four different networks were analyzed with dPC using an implementation programmed in C.

dPC group analysis

To allow comparison across the group, resultant dPC values were divided by their levels of significance (Mader et al., 2008) resulting in normalized dPC (dPC_{norm}) values. Group networks were computed by averaging these dPC_{norm} values across subjects (mean dPC_{norm}). An interaction on group level was considered significant if the following condition was fulfilled: (mean $dPC_{norm} - 2 \times stdv[mean]) > 1$.

Diffusion tensor-based probabilistic fiber tracking

Between pairs of seeds, for which a significant direct interaction was demonstrated in the dPC group analyses, intra- and interhemispheric region-to-region anatomical connectivity was computed using the method of combining probability maps (Kreher et al., 2008b). This method is ideally suited to complement the dPC analysis as it enables an extraction of the most probable direct pathway between two seed regions without using *a priori* knowledge about the presumed course.

Definition of seed regions

The same coordinates, for which dPCs were calculated, were identified in the native space of each subject's DTI by using the inverse normalization parameters obtained during the segmentation procedure of the T1 anatomical scan. These coordinates were enlarged to a sphere of 4-mm radius each containing 33 voxels. These spheres defined the seed regions for the probabilistic fiber tracking procedure.

Probabilistic diffusion tensor-based fiber tracking

DTI data were analyzed using an innovative method of pathway extraction (Kreher et al., 2008b), implemented in the Matlab-based DTI&Fiber Toolbox (http://www.uniklinik-freiburg.de/mr/live/arbeitsgruppen/diffusion_en.html). In short, we first computed the diffusion tensor (DT) (Basser et al., 1994) from the movement and distortion corrected DTI dataset. Second, a Monte Carlo simulation of Random Walks similar to the Probabilistic Index of Connectivity (PICo) method (Parker et al., 2003) was run from each seed region. Our tracking procedure differed from the classical PICo method (i) by empirically extracting the orientation density function from the DT and (ii) by preserving the main traversing direction (in relation to the first eigenvector) of each propagated trajectory during the random walk (extended probabilistic tracking, cf., Kreher et al., (2008a,b) for details). Preservation of the directional information is important for the later multiplication procedure (see below). The number of random walks was set to 10^5 and maximum fiber length to 150 voxels. The tracking area was restricted to a white matter mask to avoid tracking across anatomical borders, e.g., the lateral fissure or the cerebral falx. To ensure contact of the cortical seed regions with white matter, a rim of grey matter was included in the mask. Third, region-to-region anatomical connectivity between two seed regions was computed by combining two probability maps of interest (Kreher et al., 2008b). This combination includes a multiplication, which takes the main traversing direction of the random walk into account. Walks starting from two seed regions may either face each other (connecting fibers) or they merge and point in the same direction (merging fibers). Within the pathway connecting both seeds, the proportion of connecting fibers should exceed the proportion of merging fibers. Using the directional information (obtained by the extended probabilistic tracking) during the multiplication procedure, merging fibers are suppressed, while connecting fibers are preserved (Kreher et al., 2008b).

In the resulting combined maps, values represent a voxelwise estimation of the probability index that a voxel is part of the connecting fiber bundle of interest (in short: **p**robability **i**ndex of forming part of the **b**undle of **i**nterest, PIBI). Here, intra- and interhemispheric region-to-region anatomical connectivity was computed between pairs of seeds, for which a significant functional interaction was demonstrated in the dPC analyses.

Postprocessing of probability maps

The combined maps were scaled to the range between 0 and 1 and spatially normalized into the standard MNI space.

Group maps for each region-to-region connection were computed by averaging the combined maps from all subjects, resulting in mean maps. Consequently, voxels within these mean maps represent the arithmetic mean of the PIBI. To remove random artifacts, only voxels with PIBI values >0.0148 were displayed which excludes 95% of the voxels with $PIBI > 10^{-6}$. This value was generated empirically from the distribution observed in a large collection of preprocessed combined probability maps (Saur et al., 2008). We used a descriptive statistic rather than *t*-statistics on group level as PIBI values do not show a normal (Gaussian) distribution and no proper null hypothesis can be formulated.

Results

Network nodes revealed by SPM

Differential effects of PS relative to REV

Contrasting sound-preserved PS with sound-disturbed REV revealed five significant activation peaks in the anterior and posterior STG (T1a, T1p), the prefrontal (deep frontal operculum, FOP) and premotor cortices (pars opercularis of the inferior frontal gyrus [IFG, F3op] and dorsal premotor cortex [PMd]) (Fig. 1 and Table 1a). In the right hemisphere, activation for this contrast was only detectable after lowering the statistical threshold to $p<0.01$ uncorrected ($t>2.4$, not displayed).

Differential effects of SP relative to PS

Contrasting meaningful SP with meaningless PS revealed bilateral, left-lateralized temporofrontal activation (Fig. 1 and Table 1b). The five most significant activation peaks in the left hemisphere are located in the anterior and posterior MTG (T2a, T2p), the fusiform gyrus (FUS), and in the ventrolateral prefrontal cortex (pars orbitalis and triangularis of the IFG [F3orb, F3tri]). In the right hemisphere, homologue nodes with overall lower activation could be defined (Fig. 1 and Table 1b).

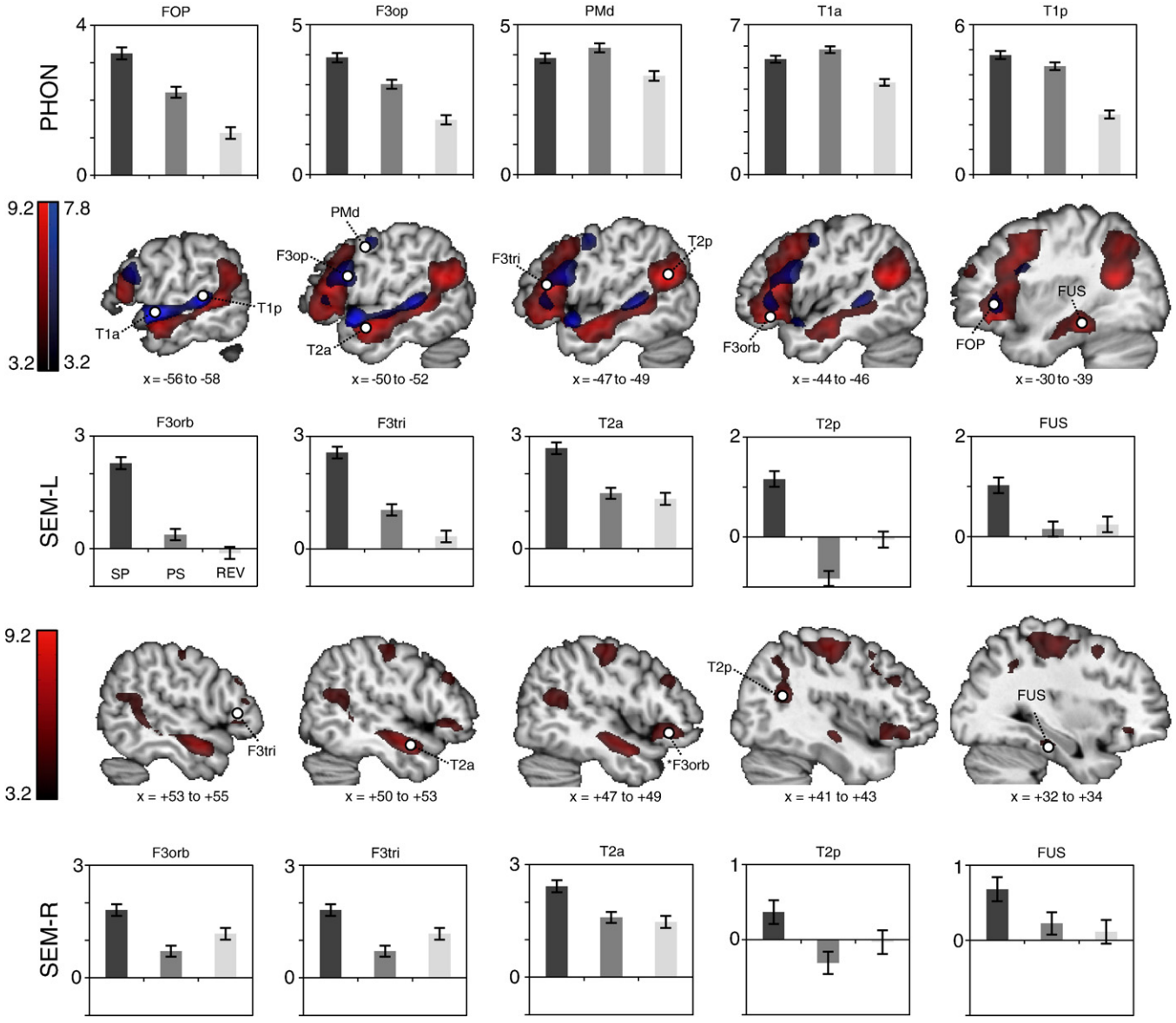

Fig. 1. Network nodes revealed by SPM. Left and right hemispheric networks subserving phonological (pseudo speech [PS] versus reversed speech [REV], blue) and semantic processing (normal speech [SP] versus pseudo speech [PS], red) identified in a random-effects analysis of 33 subjects participating in an auditory comprehension experiment. SPM *t*-maps are displayed as semitransparent maximum intensity projections in sagittal direction ($p<0.001$, uncorrected, $t>3.2$). Within major activation clusters, peak voxels defined the network nodes, indicated with a white dot. From these nodes, parameter estimates (arbitrary units) were extracted for the three conditions SP, PS, and REV and plotted as diagrams (first row: phonological nodes [PHON], second row: left semantic nodes [SEM-L]; third row: right semantic nodes [SEM-R]). Error bars indicate standard deviation of the mean. FOP, deep frontal operculum; F3op/orb/tri, pars opercularis/orbitalis/triangularis of the inferior frontal gyrus; PMd, dorsal premotor cortex; T1a/p, anterior/posterior superior temporal gyrus; T2a/p, anterior/posterior middle temporal gyrus; FUS, fusiform gyrus.

Functional network topology revealed by dPC

From these nodes, time series were extracted and analyzed in four independent networks using dPC.

The first network contained the five nodes defined by contrasting PS with REV (Fig. 2a). In this left hemispheric network (i.e., the phonological network), direct interactions were found in seven out of ten pairs of nodes (Fig. 2c). Strongest interactions were observed between neighboring nodes within the temporal (T1a–T1p) and the frontal (FOP–F3op, F3op–PMd) lobes. In addition, four long-distance temporofrontal interactions were also found significant (T1p–F3op, T1p–PMd, T1p–FOP, T1a–PMd). Using the number of interactions as a criterion, we identified the posterior temporal node (T1p) as central network node interacting with all other nodes. Notably, despite the close spatial neighborhood, the anterior temporal node (T1a) does not interact directly with the frontal operculum (FOP).

The second and third networks included those five nodes which were defined by contrasting SP with PS either in the left or right hemisphere, respectively (Fig. 2b). In these networks (i.e., the left and right semantic networks), dPC identified a significant interaction in six out of ten paired nodes in the left and in five out of ten in the right hemisphere (Fig. 2d). In both hemispheres, strongest interactions were observed between neighboring nodes within the prefrontal cortex (F3orb–F3tri). In the left hemisphere, the T2p and F3orb nodes were found as central nodes, both directly interacting with three surrounding nodes. In the right hemisphere, this central role for the T2p and F3orb nodes was not observable. Here, only the T2a node directly interacts with a frontal node (F3orb). Interestingly, in both hemispheres, nodes in the fusiform gyrus (FUS) do not directly interact with the prefrontal nodes.

Next, we analyzed left and right hemispheric nodes together in a bilateral semantic network of ten nodes. Here, strong interhemispheric

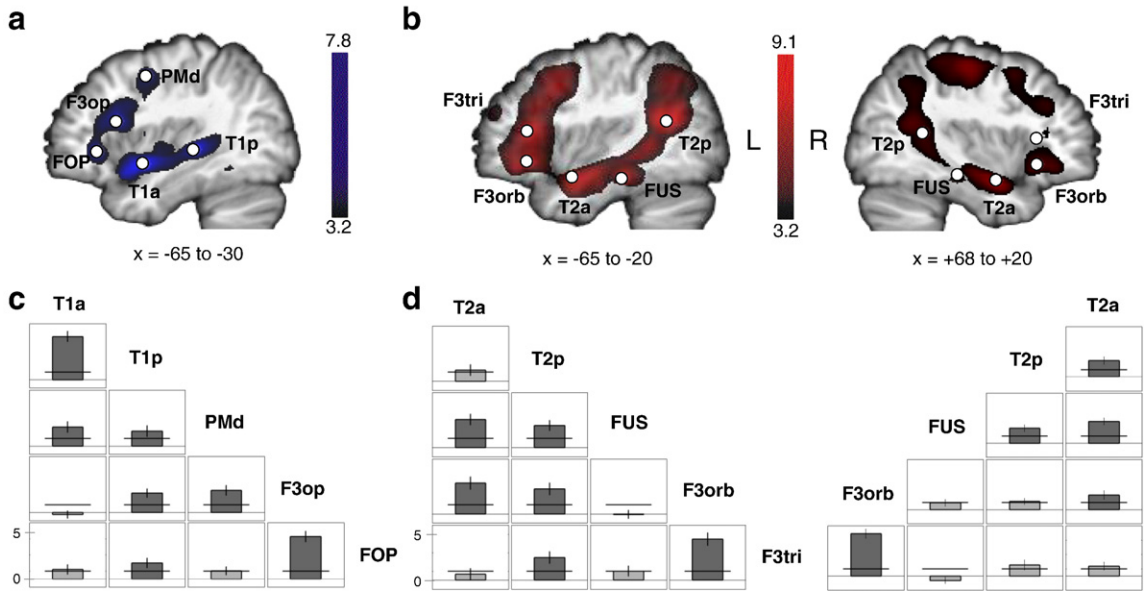

Fig. 2. Functional connectivity in the phonological and semantic networks revealed by dPC. In the upper row, networks subserving phonological (a) and semantic (b) processing are displayed as maximum intensity projections in sagittal direction ($p<0.001$, uncorrected, $t>3.2$). In the lower row, mean directed partial correlation (dPC) values are plotted for each pairwise interaction within the left phonological (c) and left and right semantic (d) networks, respectively. An interaction was defined significant if the mean dPC value minus two standard deviations of the mean (indicated by the error bar) were larger than 1 (indicated by the horizontal line). Significant interactions are displayed as dark grey plots. Abbreviations are as indicated in Fig. 1.

interactions were exclusively detected between homotopic temporal and frontal nodes (Fig. 3). These strong interhemispheric interactions dominate the network structure in a way that some of the intra-hemispheric interactions, which were significant in the separate analyses of the left and right semantic nodes, disappear (left FUS–T2p, FUS–T2a, right FUS–T1p, FUS–T1a, T1a–F3orb). However, no additional interactions within both hemispheres were detected.

To verify our results, an ordinary partial correlation analysis was performed. All connections revealed by dPC analysis were detected by ordinary partial correlation analysis, too. The latter, however, detected additional interactions (see Tables 1–4 in the supplementary results). A simulation study (not shown) has demonstrated that ordinary partial correlation analysis leads to false-positive interactions in addition to the present ones.

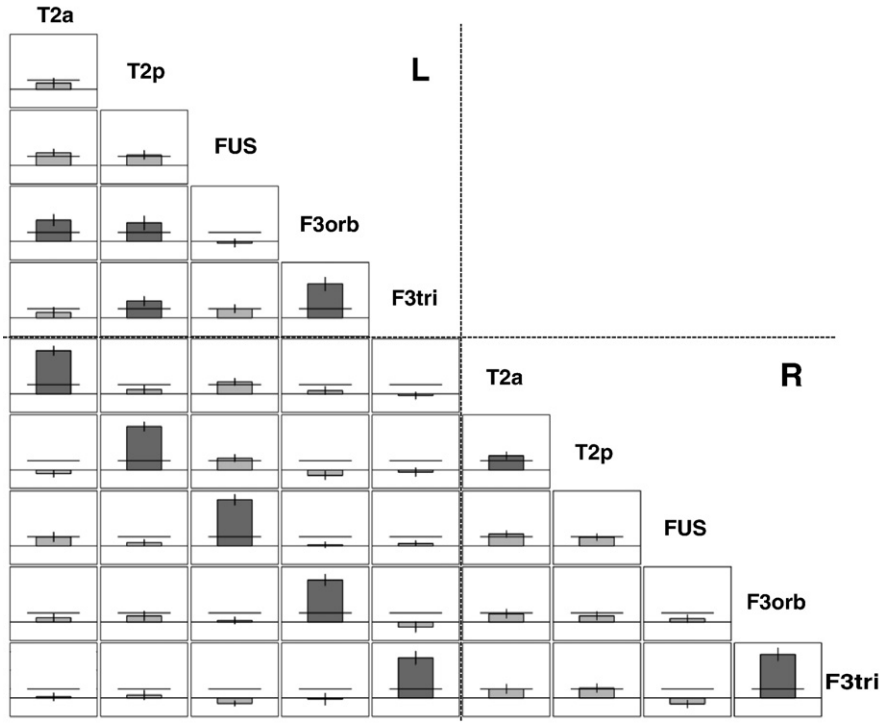

Fig. 3. Functional connectivity within the bilateral semantic network revealed by dPC. Mean directed partial correlation (dPC) values are plotted for each pairwise interaction within the bilateral semantic network. Please note the strong functional interactions between homotopic nodes of the left and right hemispheres (diagonal in the left lower quadrant). Abbreviations are as indicated in Fig. 1.

Anatomical network topology revealed by probabilistic tractography

For each pairwise interaction, which showed a direct interaction in the dPC analysis, we extracted region-to-region anatomical pathways by combining probability maps from the respective nodes.

In the phonological network, fibers mediating long-distance interactions between the temporal (T1a, T1p) and the premotor nodes (F3op, PMd) were found to take a dorsal route via the superior longitudinal and arcuate fascicles (SLF/AF system, Figs. 4a and b). In contrast, interaction between T1p and the prefrontal node (FOP) is mediated by a ventral route via the extreme capsule (EmC, Figs. 4d and e). Within the temporal lobe, the interaction between the anterior and posterior STG is enabled by the middle longitudinal fascicle (MdLF) (Fig. 4c). Within the frontal lobe, functional interaction between adjacent prefrontal and premotor nodes is mediated by short association fibers (Fig. 4f, 1–2).

In the left and right semantic networks, long-distance interactions between temporal (T2a, T2p) and prefrontal nodes (F3orb, F3tri) are exclusively mediated via the ventral pathway through the EmC (Figs. 5a–c and 6a and b). In the right temporal lobe, MdLF enables interaction between the anterior and posterior MTG (Fig. 6c). In both hemispheres, the fusiform node (FUS) interacts with T2p via the inferior longitudinal fascicle (ILF, Figs. 5e and 6e) and with T2a via a connection which first runs in posterior direction in the ILF before turning around and joining the MdLF in an anterior direction (Figs. 5f and 6f). Within the left and right prefrontal lobe, adjacent nodes interact via short association fibers (Figs. 5d and 6d).

In the bilateral semantic network (Fig. 3), strong functional interactions between homotopic nodes were observed. These interhemispheric interactions were shown to be mediated by distinct commissural fibers (Fig. 7). Interactions between both F3orb nodes are conveyed via commissural fibers running through the genu of the corpus callosum (CC) anteriorly to fibers connecting both F3tri nodes (Figs. 7a–d). In contrast, interactions between homotopic temporal nodes are mediated by commissural fibers running through the splenium of the CC. Within the splenium, a spatial alignment of fibers was found, too. For the fusiform nodes, transcallosal fibers run inferiorly to fibers from the middle temporal nodes (Figs. 7a, b, e–g).

Fig. 8 summarizes the findings of the functional and structural network analyses. Networks attributed to phonological and semantic processing are displayed as schematic diagrams: Functional interactions as revealed by dPC were drawn with the knowledge of the most probable anatomical course of the underlying white matter fiber tracts as revealed by fiber tracking.

Discussion

In this study, we introduce a novel combination of functional and structural connectivity which is capable of describing large-scale cognitive brain networks. In contrast to a recent suggestion by Stephan et al. (2009) who constrained their models of effective connectivity by instilling anatomical information derived from probabilistic fiber tracking, we here constrained a region-to-region probabilistic tractography with the results from the functional connectivity analysis to identify the fiber tracts most likely mediating the functional interactions. Exemplarily, we applied this combined approach to the data of an auditory language comprehension experiment to describe the specific functional and anatomical network characteristics of two distinct processing levels. We first discuss issues concerning the employed methods followed by a functional discussion of the networks.

Methodological issues

The nodes of the networks were selected based on the contrasts either between PS and REV or SP and PS. The selection of nodes is a critical step in every kind of network analysis, irrespective of the underlying computational method. Here we decided to select the major language-relevant clusters in both contrasts. If essential nodes characterizing the differences between the two conditions are missing, false conclusions might arise. However, we believe that our selection is representative for both contrasts and best reflects the cognitive processes of interest. Having defined the nodes, subsequent

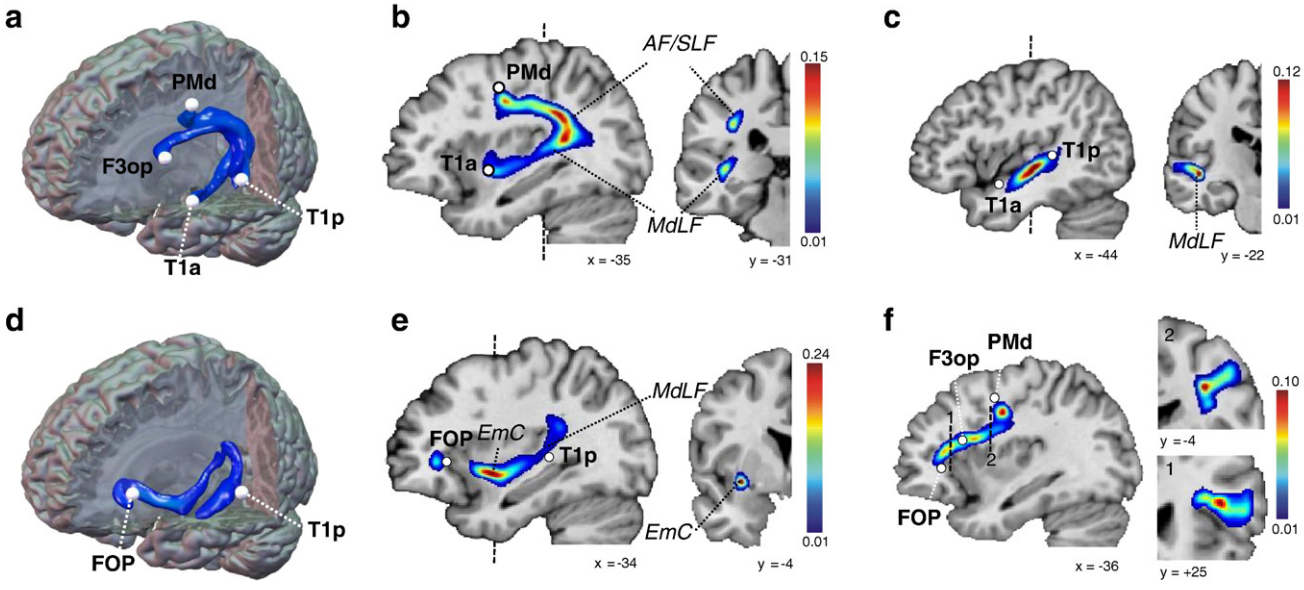

Fig. 4. Fiber tracts mediating functional connectivity in the phonological network. Long (a–e) and short (f) association fibers connecting functionally interacting nodes in the phonological network as revealed by probabilistic tractography. The color coding represents the mean PIBI value (probability index forming part of the bundle of interest, see Methods) across 33 subjects; the value at the top of the color bar represents the maximum mean PIBI value for each connection. Dashed, vertical lines indicate the level of the coronal sections. Three dimensional (3D) rendering in panel a illustrates the spatial course of all three dorsal temporofrontal connections (i.e., T1a–PMd [displayed as section in panel b], T1p–PMd, T1p–F3op). Rendering in panel d illustrates the ventral temporofrontal connection between T1p and FOP (shown as section in panel e). Colors in the 3D renderings are optimized for spatial visualization and do not represent a quantitative estimation. AF/SLF, arcuate/superior longitudinal fascicle; EmC, extreme capsule; MdLF, middle longitudinal fascicle; abbreviations of network nodes are as indicated in Fig. 1.

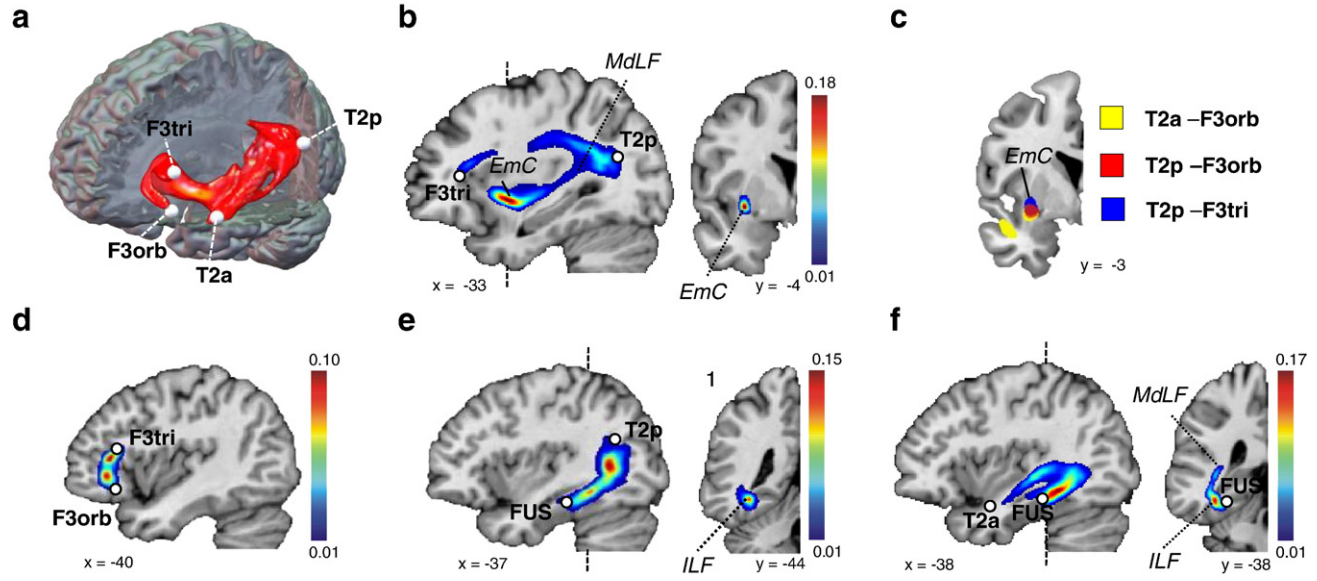

Fig. 5. Fiber tracts mediating functional connectivity in the left semantic network. Long (a,b, e,f) and short (d) association fibers connecting functionally interacting nodes in the left semantic network as revealed by probabilistic tractography. The three-dimensional rendering in panel a illustrates the spatial course of all three ventral temporofrontal connections (i.e., T2a–F3orb, T2p–F3orb, T2p–F3tri [displayed as section in panel b]). An overlay of these connections shows that all fibers run through the EmC, with some degree of spatial segregation (c). EmC, extreme capsule; MdLF, middle longitudinal fascicle; ILF, inferior longitudinal fascicle. Abbreviations of network nodes are as indicated in Fig. 1.

analysis of the functional and anatomical network architecture was fully data-driven and required no further *a priori* hypothesis.

From a computational point of view, the crucial characteristic of the dPC analysis is that it takes the past of the processes into account. If temporal resolution is high, e.g., in EEG or MEG measurements, delays in the signal between regions allow for the detection of directed (causal) interdependencies (i.e., "effective connectivity"). However, in the case of fMRI with sampling rates of about 2 s, interactions must be regarded as instantaneous, thus information of the past cannot be used to explain the direction of information flow. With reference to the imaging terminology (Stephan, 2004), using the dPC method, we computed "functional connectivity," i.e., undirected interactions among areas. The problem of poor temporal resolution of fMRI time series, however, is not a drawback specific to the dPC method but rather concerns all network identification procedures when applied to fMRI data. In contrast to dPC, which infers connectivity directly from the BOLD time series, other network identification procedures like dynamic causal modeling (DCM) (Friston et al., 2003) perform a deconvolution procedure of the BOLD data to estimate connectivity at the neuronal level. Directed interactions therefore are assumed to be detectable independent from delays in the BOLD signal. Using a deconvolution procedure, however, does not increase the temporal resolution per se. It is therefore questionable to which extent the analysis on the neuronal level does contain the information necessary to determine causal inferences.

Despite this shortcoming due to the temporal properties of the fMRI data, the consideration of the processes' past has a major advantage, which makes dPC a valuable tool in deducing functional

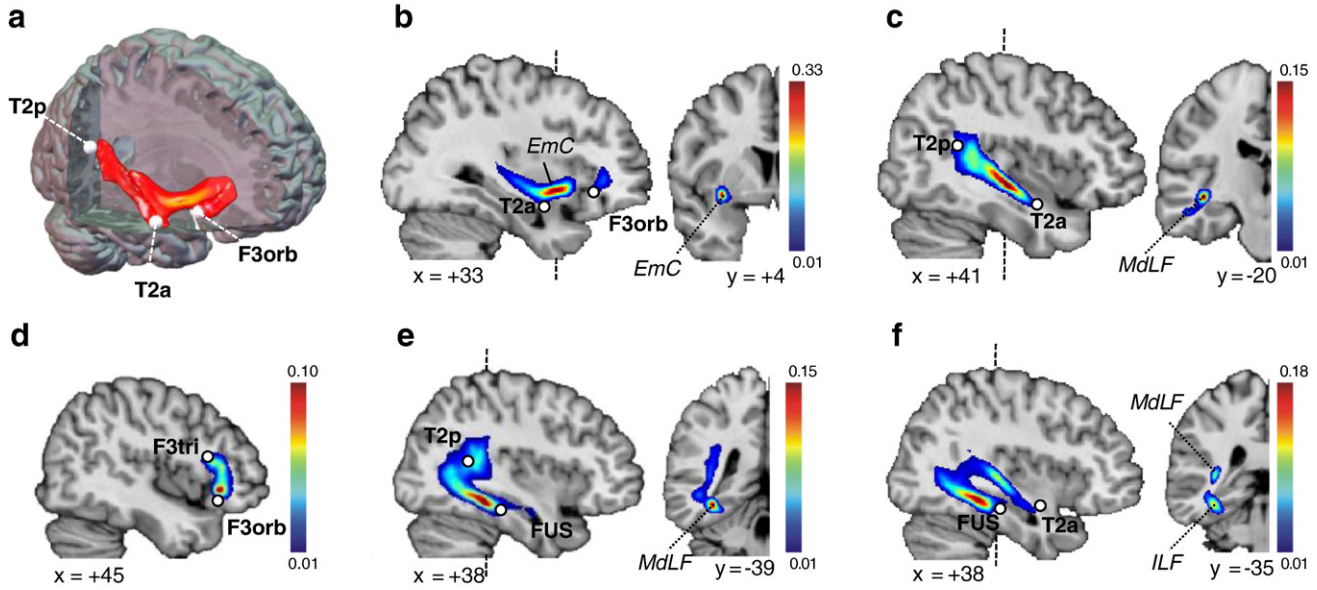

Fig. 6. Fiber tracts mediating functional connectivity in the right semantic network. Long (a–c, e–f) and short (d) association fibers connecting functionally interacting nodes in the right semantic network. The three-dimensional rendering in panel a illustrates the spatial course of the connections displayed in panels b and c. EmC, extreme capsule; MdLF, middle longitudinal fascicle; ILF, inferior longitudinal fascicle. Abbreviations of network nodes are as indicated in Fig. 1.

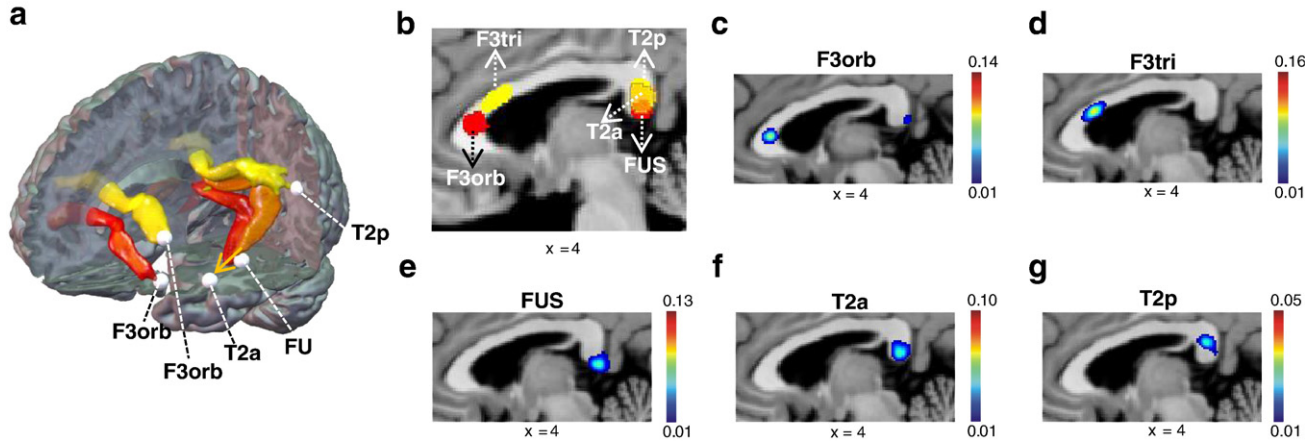

Fig. 7. Commissural fibers mediating interhemispheric connectivity between homotopic nodes. Commissural fibers passing through the midsagittal plane of the corpus callosum (CC) mediating interhemispheric interactions between homotopic nodes. Panel a illustrates the spatial course of all five commissural fibers; panel b summarizes the topography of the CC by an overlay of binary maps of all five commissural tracts. Abbreviations of network nodes are as indicated in Fig. 1.

connectivity from fMRI data. It ensures that contributions that can directly be explained from the processes' past do not influence the results of instantaneous connection estimation which reduces the number of false-positive/negative conclusions. For example, false-*positive* interactions might arise from blood flow patterns that are independent from neural activity. Strong resting state correlations have been reported between homotopic brain regions which might – at least partly – be explained by the symmetry between the blood supply routes of homologues regions (Hampson et al., 2002). Give that dPC are more likely to diminish those task irrelevant fluctuations than other techniques, the strong interhemispheric interactions between homotopic nodes in our analysis are considered as task relevant interactions. In contrast, false-*negative* interactions in ordinary correlation-based techniques might result, e.g., from inter-regional variability of the HRF's shape (e.g., onset-delay) despite similar neuronal activity (Sun et al., 2004).

For directly interacting pairs of nodes, a region-to-region probabilistic fiber tracking (Kreher et al., 2008b) was performed to visualize the most probable white matter fiber tracts mediating these interactions. That is, prior functional network analysis restricts the fiber tracking to task-relevant interactions which represents an important advancement to recent studies combining fMRI and DTI (Friederici et al., 2006; Parker et al., 2005; Saur et al., 2008).

We first computed one-sided probability maps from each network node. The resulting maps represent a probability measure for the visited voxels to be connected with the start voxel. To get region-to-region anatomical connectivity, we multiplied those maps, for which a direct interaction was found in the dPC analysis. This multiplication takes the directional information of the random walks into account which allows for distinguishing connecting from merging fibers. This approach enables a highly efficient detection of the most probable anatomical connection – even if seed regions are small and distances are long – without *a priori* knowledge concerning the presumed course of the connection. Owing to the multiplication step, this kind of tracking is most sensitive to the midsection of a connection since here, despite distance effects, probabilities are still high for both seed regions. Notably, the region-to-region fiber tracking does not necessarily demonstrate the existence of a monosynaptic anatomical connection between two nodes but rather visualizes the most probable anatomical course along which the functional interaction might be mediated.

The dPC and fiber tracking are both independent but complementary in the sense that the demonstration of a functional interaction supports the functional relevance of the anatomical connection and vice versa. This is especially important since one might argue that the detected functional interactions (partly) arise from a third, unidentified region. Converging evidence from two independent methods therefore foster the significance of the resulting networks.

Although it might be straightforward to relate functional (e.g., dPC values) and anatomical (e.g., PIBI values) connection strengths to each other, those ideas must be taken with great caution as a quantitative comparison between different probabilistic tracts so far is difficult. This is because PIBI values depend on many parameters such as anatomical properties of the fiber tract (e.g., consider the EmC which typically shows high PIBI values at the level of the insular cortex due to high fiber alignment), partial volume effects (i.e., each voxel contains a different texture of fibers, neural and glial tissue), noise in the DTI data, as well as distance effects (i.e., the visiting frequency decreases with increasing distance to the seed region). The lack of

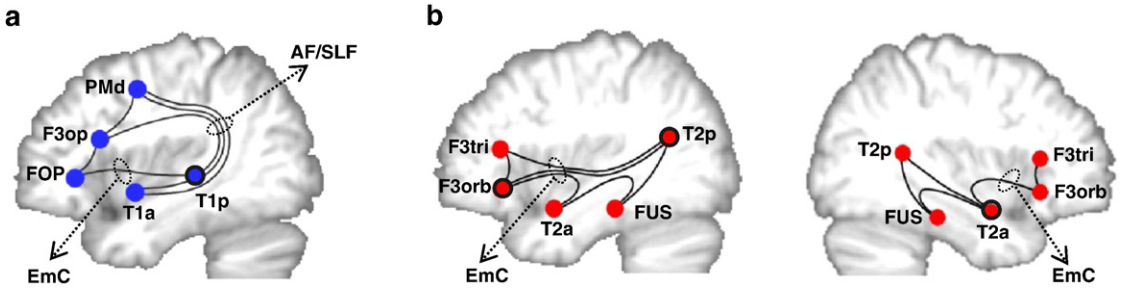

Fig. 8. Functionally and anatomically defined networks subserving phonological (a) and semantic (b) processing. Schematics of the networks evaluated with directed partial correlation (dPC) and probabilistic fiber tracking. Black lines indicate significant functional interactions as revealed by dPC which are drawn with the knowledge of the anatomical course as identified by tractography. Central nodes within the networks (indicated with a black circle) are defined by their number of interactions. AF/SLF, arcuate/superior longitudinal fascicle; EmC, extreme capsule.

quantification of fiber tracking results is a matter of great discussion and maybe overcome by novel fiber tracking techniques, e.g., global tracking of white matter as in the recently suggested Gibbs tracking (Kreher et al., 2008a) as well as MR developments which improve the spatial resolution of DTI.

Functional interpretation

We characterized two levels of auditory language comprehension: a lower level of speech perception, mainly engaged in phonological processing and a higher level of speech recognition, mainly attributable to semantic processing. This differentiation might be criticized as linguistically underspecified. For example, one might argue that reversed speech contains legal phonemes as well (see Scott and Wise (2004) for a comprehensive review on this issue) and thus, the phonological condition might be underestimated. Or, the experiment does not sufficiently control for syntactic or prosodic features. However, it distinguishes reasonably two processing levels in natural auditory language comprehension which are characterized by highly plausible functional and anatomical network characteristics.

Within the network attributed to phonological processing, the node in the posterior STG directly interacts with all other nodes and thus was identified as a central node. This is in agreement with a number of previous findings emphasizing the importance of the posterior STG in early auditory stages of sound-to-meaning transformation, or, more specifically, in phonetic discrimination (Buchsbaum et al., 2001; Burton et al., 2005; Demonet et al., 2005; Jacquemot et al., 2003; Nadeau, 2001; Vigneau et al., 2006). However, none of these studies explicitly related this central role to its functional and anatomical connections to other areas. Here, we showed that the posterior STG exhibits extensive direct interactions with all frontal nodes. With the premotor nodes, this interaction is mediated via the dorsal AF/SLF system (Frey et al., 2008; Saur et al., 2008). This temporo–premotor interaction via the dorsal pathway is important for a rapid, automated conversion of acoustic representations into motor representations (Liberman and Whalen, 2000; Nadeau, 2001; Vigneau et al., 2006). Thus, phonetic discrimination during speech perception depends not only on acoustically based processes in superior temporal areas but rather is achieved through the simulation of the motor response within an interacting system of temporal association and frontal premotor cortices (Liberman's "motor theory of speech" (Liberman and Whalen, 2000)). This view is directly supported by our previous study (Saur et al., 2008) in which we showed that sublexical repetition of pseudowords involves a quite similar temporofrontal network.

In contrast, interaction with the deep frontal operculum (FOP) in the prefrontal cortex is mediated via the ventral EmC/MdLF system (Frey et al., 2008; Saur et al., 2008). The FOP, in turn, strongly interacts with the premotor nodes via short association fibers (Schmahmann et al., 2008). We suggest that this indirect interaction of the STG with premotor regions via the FOP is important for controlling the dorsal sensory–motor loop during speech perception.

Within the left semantic network, the node in the posterior MTG (T2p) directly interacts with both prefrontal nodes and the F3orb node directly interacts with both middle temporal nodes. This identified these nodes as central relay stations in the left semantic network. By taking into consideration the specialization for different aspects of semantic processing of the participating regions, the posterior MTG (and neighboring parts of the ITG) is proposed to store and provide access to lexical–semantic representations (Crinion et al., 2003; Hickok and Poeppel, 2004, 2007; Leff et al., 2008). Via the ventral MdLF/EmC system (Frey et al., 2008; Saur et al., 2008), the middle temporal nodes interact with the prefrontal nodes. These tight functional and anatomical interactions between temporal and ventrolateral prefrontal areas are essential for contextual integration (Dapretto and Bookheimer, 1999; Kaan and Swaab, 2002), controlled retrieval (Thompson-Schill et al., 1997), and selection (Rodd et al., 2005) of lexical information and relation of linguistic meaning to stored knowledge about the world (Hagoort et al., 2004). MEG studies have shown that about 90 ms after auditory presentation of a spoken word, a temporal source starts to build up while a prefrontal source appears later, after about 120 ms (Pulvermuller et al., 2003). The integration of this temporal information into our left semantic network model (Fig. 8b) leads to the conclusion that the direction of information flow during auditory comprehension runs from temporal to frontal (cf., also Leff et al., 2008). That is, during auditory comprehension, the posterior temporal cortex exerts influence upon prefrontal regions via both, direct and indirect interactions via inferior temporal and anterior temporal regions.

Activations in the right hemisphere were weaker but essentially mirrored those in the left. By analyzing the time series of left and right semantic nodes in a single network, we found strong functional interactions between all homotopic nodes. These interhemispheric interactions are mediated by distinct commissural fibers crossing through the genu (linking bilateral PFC) and splenium (linking bilateral temporal cortex) of the corpus callosum. This topography is in accordance with tract tracing studies in monkeys (Schmahmann and Pandya, 2006) and a DTI-based parcellation study of the human callosum (Huang et al., 2005). Together, these complementary results are consistent with a bilateral, parallel operating network for semantic processing in which the right hemisphere performs computations for the same general processes as the left. According to Jung-Beeman (2005), in the right hemisphere, these computations might be less finely tuned. The hypothesis of a bilateral, parallel processing language network is also supported by the observation that homologue right hemisphere language areas contribute to language recovery in patients with left hemispheric lesions (Crinion and Price, 2005; Leff et al., 2002; Saur et al., 2006; Weiller et al., 1995).

Here, we experimentally segregated phonological and semantic processing steps to identify the functional and anatomical characteristics of these subsystems. Nevertheless, we are aware that it is not universally accepted that an explicit sublexical perceptual level exists which identifies phonemes *after* acoustic analysis and *prior* to lexical activation (Scott and Wise, 2004). Rather, it is more likely that in natural language comprehension, both processes work in parallel and influence each other (McClelland and Rogers, 2003).

In summary, the combination of functional and anatomical connectivity represents a promising approach to describe how specific cognitive operations emerge through interaction between anatomically interconnected brain areas. This type of analysis should be applied to patients with focal brain lesions, e.g., due to ischemic stroke. We postulate that central network nodes as identified by dPC represent those brain areas, to which damage causes a network disruption associated with a severe language deficit ("concept of the critical lesion"). It would therefore be of great interest to see how real (in case of, e.g., stroke) or virtual (e.g., using transcranial magnetic stimulation) disruption of particular network components alters the network structure, or, depending on the lesion, how well the functional deficit might be predicted by these networks.

Acknowledgments

The work was supported by the Federal Ministry of Education and Research (BMBF-research collaborations "Mechanisms of brain reorganization in the language network" [01GW0661] and "Neuroimaging Centers" [01GO0513]), the German Research Foundation (WE1352/14-1), and the Excellence Initiative of the German federal and state governments.

Appendix A. Supplementary data

Supplementary data associated with this article can be found, in the online version, at doi:10.1016/j.neuroimage.2009.11.009.

References

Ashburner, J., Friston, K.J., 2005. Unified segmentation. Neuroimage 26, 839–851.

Baccala, L.A., Sameshima, K., 2001. Partial directed coherence: a new concept in neural structure determination. Biol. Cybern. 84, 463–474.

Basser, P.J., Mattiello, J., LeBihan, D., 1994. Estimation of the effective self-diffusion tensor from the NMR spin echo. J. Magn. Reson. B 103, 247–254.

Bitan, T., Booth, J.R., Choy, J., Burman, D.D., Gitelman, D.R., Mesulam, M.M., 2005. Shifts of effective connectivity within a language network during rhyming and spelling. J. Neurosci. 25, 5397–5403.

Buchsbaum, B.R., Hickok, G., Humphries, C., 2001. Role of left posterior superior temporal gyrus in phonological processing for speech perception and production. Cognitive Science 25, 663–678.

Burton, M.W., Locasto, P.C., Krebs-Noble, D., Gullapalli, R.P., 2005. A systematic investigation of the functional neuroanatomy of auditory and visual phonological processing. Neuroimage 26, 647–661.

Crinion, J., Price, C.J., 2005. Right anterior superior temporal activation predicts auditory sentence comprehension following aphasic stroke. Brain 128, 2858–2871.

Crinion, J.T., Lambon-Ralph, M.A., Warburton, E.A., Howard, D., Wise, R.J., 2003. Temporal lobe regions engaged during normal speech comprehension. Brain 126, 1193–1201.

Dapretto, M., Bookheimer, S.Y., 1999. Form and content: dissociating syntax and semantics in sentence comprehension. Neuron 24, 427–432.

Demonet, J.F., Thierry, G., Cardebat, D., 2005. Renewal of the neurophysiology of language: functional neuroimaging. Physiol. Rev. 85, 49–95.

Dhamala, M., Rangarajan, G., Ding, M., 2008. Analyzing information flow in brain networks with nonparametric Granger causality. Neuroimage 41, 354–362.

Eichler, M., 2005. A graphical approach for evaluating effective connectivity in neural systems. Philos. Trans. R Soc. Lond. B. Biol. Sci. 360, 953–967.

Frey, S., Campbell, J.S., Pike, G.B., Petrides, M., 2008. Dissociating the human language pathways with high angular resolution diffusion fiber tractography. J. Neurosci. 28, 11435–11444.

Friederici, A.D., Bahlmann, J., Heim, S., Schubotz, R.I., Anwander, A., 2006. The brain differentiates human and non-human grammars: functional localization and structural connectivity. Proc. Natl. Acad. Sci. U. S. A. 103, 2458–2463.

Friston, K.J., Harrison, L., Penny, W., 2003. Dynamic causal modelling. Neuroimage 19, 1273–1302.

Granger, J., 1969. Investigating causal relations by econometric models and cross-spectral methods. Econometrica 37, 424–438.

Hagoort, P., Hald, L., Bastiaansen, M., Petersson, K.M., 2004. Integration of word meaning and world knowledge in language comprehension. Science 304, 438–441.

Hampson, M., Peterson, B.S., Skudlarski, P., Gatenby, J.C., Gore, J.C., 2002. Detection of functional connectivity using temporal correlations in MR images. Hum. Brain Mapp. 15, 247–262.

Heim, S., Eickhoff, S.B., Ischebeck, A.K., Friederici, A.D., Stephan, K.E., Amunts, K., 2009. Effective connectivity of the left BA 44, BA 45, and inferior temporal gyrus during lexical and phonological decisions identified with DCM. Hum. Brain Mapp. 30, 392–402.

Hickok, G., Poeppel, D., 2004. Dorsal and ventral streams: a framework for understanding aspects of the functional anatomy of language. Cognition 92, 67–99.

Hickok, G., Poeppel, D., 2007. The cortical organization of speech processing. Nat. Rev. Neurosci. 8, 393–402.

Huang, H., Zhang, J., Jiang, H., Wakana, S., Poetscher, L., Miller, M.I., van Zijl, P.C., Hillis, A.E., Wytik, R., Mori, S., 2005. DTI tractography based parcellation of white matter: application to the mid-sagittal morphology of corpus callosum. Neuroimage 26, 195–205.

Jacquemot, C., Pallier, C., LeBihan, D., Dehaene, S., Dupoux, E., 2003. Phonological grammar shapes the auditory cortex: a functional magnetic resonance imaging study. J. Neurosci. 23, 9541–9546.

Jung-Beeman, M., 2005. Bilateral brain processes for comprehending natural language. Trends Cogn. Sci. 9, 512–518.

Kaan, E., Swaab, T.Y., 2002. The brain circuitry of syntactic comprehension. Trends Cogn. Sci. 6, 350–356.

Kayser, A.S., Sun, F.T., D'Esposito, M., 2009. A comparison of Granger causality and coherency in fMRI-based analysis of the motor system. Hum. Brain Mapp. 30, 3475–3494.

Keil, A., Sabatinelli, D., Ding, M., Lang, P.J., Ihssen, N., Heim, S., 2009. Re-entrant projections modulate visual cortex in affective perception: evidence from Granger causality analysis. Hum. Brain Mapp. 30, 532–540.

Kreher, B.W., Mader, I., Kiselev, V.G., 2008a. Gibbs tracking: a novel approach for the reconstruction of neuronal pathways. Magn. Reson. Med. 60, 953–963.

Kreher, B.W., Schnell, S., Mader, I., Il'yasov, K.A., Hennig, J., Kiselev, V.G., Saur, D., 2008b. Connecting and merging fibres: pathway extraction by combining probability maps. Neuroimage 43, 81–89.

Leff, A., Crinion, J., Scott, S., Turkheimer, F., Howard, D., Wise, R., 2002. A physiological change in the homotopic cortex following left posterior temporal lobe infarction. Ann. Neurol. 51, 553–558.

Leff, A.P., Schofield, T.M., Stephan, K.E., Crinion, J.T., Friston, K.J., Price, C.J., 2008. The cortical dynamics of intelligible speech. J. Neurosci. 28, 13209–13215.

Liberman, A.M., Whalen, D.H., 2000. On the relation of speech to language. Trends Cogn. Sci. 4, 187–196.

Mader, W., Feess, D., Lange, R., Saur, D., Glauche, V., Weiller, C., Timmer, J., Schelter, B., 2008. On the detection of direct directed information flow in fMRI. IEEE Journal of Selected Topics in Signal Processing 2, 965–974.

McClelland, J.L., Rogers, T.T., 2003. The parallel distributed processing approach to semantic cognition. Nat. Rev. Neurosci. 4, 310–322.

Mechelli, A., Crinion, J.T., Long, S., Friston, K.J., Lambon Ralph, M.A., Patterson, K., McClelland, J.L., Price, C.J., 2005. Dissociating reading processes on the basis of neuronal interactions. J. Cogn. Neurosci. 17, 1753–1765.

Mesulam, M.M., 1990. Large-scale neurocognitive networks and distributed processing for attention, language, and memory. Ann. Neurol. 28, 597–613.

Nadeau, S.E., 2001. Phonology: a review and proposals from a connectionist perspective. Brain Lang. 79, 511–579.

Parker, G.J., Haroon, H.A., Wheeler-Kingshott, C.A., 2003. A framework for a streamline-based probabilistic index of connectivity (PICo) using a structural interpretation of MRI diffusion measurements. J. Magn. Reson. Imaging 18, 242–254.

Parker, G.J., Luzzi, S., Alexander, D.C., Wheeler-Kingshott, C.A., Ciccarelli, O., Lambon Ralph, M.A., 2005. Lateralization of ventral and dorsal auditory–language pathways in the human brain. Neuroimage 24, 656–666.

Pulvermuller, F., Shtyrov, Y., Ilmoniemi, R., 2003. Spatiotemporal dynamics of neural language processing: an MEG study using minimum-norm current estimates. Neuroimage 20, 1020–1025.

Rodd, J.M., Davis, M.H., Johnsrude, I.S., 2005. The neural mechanisms of speech comprehension: fMRI studies of semantic ambiguity. Cereb. Cortex 15, 1261–1269.

Roebroeck, A., Formisano, E., Goebel, R., 2005. Mapping directed influence over the brain using Granger causality and fMRI. Neuroimage 25, 230–242.

Saur, D., Kreher, B.W., Schnell, S., Kummerer, D., Kellmeyer, P., Vry, M.S., Umarova, R., Musso, M., Glauche, V., Abel, S., Huber, W., Rijntjes, M., Hennig, J., Weiller, C., 2008. Ventral and dorsal pathways for language. Proc. Natl. Acad. Sci. U. S. A. 105, 18035–18040.

Saur, D., Lange, R., Baumgaertner, A., Schraknepper, V., Willmes, K., Rijntjes, M., Weiller, C., 2006. Dynamics of language reorganization after stroke. Brain 129, 1371–1384.

Schmahmann, J.D., Pandya, D.N., 2006. Fiber Pathways of the Brain. Oxford University Press, New York.

Schmahmann, J.D., Smith, E.E., Eichler, F.S., Filley, C.M., 2008. Cerebral white matter: neuroanatomy, clinical neurology, and neurobehavioral correlates. Ann. N. Y. Acad. Sci. 1142, 266–309.

Scott, S.K., Wise, R.J.S., 2004. The functional neuroanatomy of prelexical processing in speech perception. Cognition 92, 13–45.

Stephan, K.E., 2004. On the role of general system theory for functional neuroimaging. J. Anat. 205, 443–470.

Stephan, K.E., Tittgemeyer, M., Knosche, T.R., Moran, R.J., Friston, K.J., 2009. Tractography-based priors for dynamic causal models. Neuroimage 47, 1628–1638.

Sun, F.T., Miller, L.M., D'Esposito, M., 2004. Measuring interregional functional connectivity using coherence and partial coherence analyses of fMRI data. Neuroimage 21, 647–658.

Thompson-Schill, S.L., D'Esposito, M., Aguirre, G.K., Farah, M.J., 1997. Role of left inferior prefrontal cortex in retrieval of semantic knowledge: a reevaluation. Proc. Natl. Acad. Sci. U. S. A. 94, 14792–14797.

Vigneau, M., Beaucousin, V., Herve, P.Y., Duffau, H., Crivello, F., Houde, O., Mazoyer, B., Tzourio-Mazoyer, N., 2006. Meta-analyzing left hemisphere language areas: phonology, semantics, and sentence processing. Neuroimage 30, 1414–1432.

Weiller, C., Isensee, C., Rijntjes, M., Huber, W., Muller, S., Bier, D., Dutschka, K., Woods, R. P., Noth, J., Diener, H.C., 1995. Recovery from Wernicke's aphasia: a positron emission tomographic study. Ann. Neurol. 37, 723–732.

Zaitsev, M., Hennig, J., Speck, O., 2004. Point spread function mapping with parallel imaging techniques and high acceleration factors: fast, robust, and flexible method for echo-planar imaging distortion correction. Magn. Reson. Med. 52, 1156–1166.